THE ASTROPHYSICAL JOURNAL, 467:811–818, 1996 August 20

ORBITAL DECAY, SPIN-DOWN, AND PULSE-PHASE RESOLVED-SPECTROSCOPY OF LMC X-4 FROM *GINGA* AND *ROSAT* OBSERVATIONS

JONATHAN W. WOO,[1] GEORGE W. CLARK,[2] AND ALAN M. LEVINE
Center for Space Research, Massachusetts Institute of Technology, Cambridge, MA 02139
ROBIN H. D. CORBET[3]
Laboratory for High Energy Astrophysics, NASA/Goddard Space Flight Center, Greenbelt, MD 20771
AND
FUMIAKI NAGASE
The Institute of Space and Astronautical Science, 3-1-1 Yoshinodai, Sagamihara, Kanagawa 229, Japan
Received 1995 December 8; accepted 1996 March 8

ABSTRACT

We report pulse-timing and pulse-phase resolved spectrum analysis of LMC X-4 observations by the X-ray satellites *Ginga* in 1988 and *ROSAT* in 1991 extending over a combined energy range from 0.2 to 37 keV. The results, when combined with previous results of X-ray observations dating back to 1977, yield marginal evidence of orbital decay with an average rate of change in the orbital period of $\dot{P}_{\rm orb}/P_{\rm orb} = (-5.3 \pm 2.7) \times 10^{-7}$ yr^{-1}. This low decay rate and the relatively small radius of the companion point to the conclusion that the companion is still in the hydrogen core-burning stage of its evolution. The pulse period increased between the two observations at an average rate of $\dot{P}_{\rm pulse} = (1.91 \pm 0.01) \times 10^{-3}$ s yr^{-1}. At other times, the spin period has both decreased and increased. The neutron star must therefore be in the condition of approximate spin equilibrium wherein its period is close to the Kepler period at the inner edge of the accretion disk. For a disk-accreting pulsar with the luminosity ($\sim 10^{38.6}$ ergs s^{-1}) and spin period ($\sim$13.5 s) of LMC X-4, this condition implies that its magnetic dipole moment is exceptionally large, of the order of $10^{31.5}$ G cm^3. The pulse-phase resolved combined pulse-height distributions are well fitted with a model spectrum consisting of the sum of four components, a Planck function (PF), thermal bremsstrahlung (TB), power law (PL), and iron K-line (FE), multiplied by a photoelectric absorption factor, an exponential high-energy cutoff and a cyclotron resonance attenuation factor. The pulse profiles of the TB and PL ($E > 15$ keV) energy fluxes are single-peaked with pulse fractions of $\sim$0.12 and $\sim$0.16, respectively, but $\sim 180°$ different in phase. The Fe-line flux also exhibits a single peak pulse profile. Its pulse fraction is $\sim$0.37, and its peak lags that of the PL peak by $\sim 140°$. The PL ($E > 15$ keV) profile is attributed to a pencil-beam–like anisotropy in the emission and the TB profile to a fan-beam-like anisotropy with the condition that the sum of the spin axis inclination and the angle between the spin and magnetic dipole axes is less than 90°. The PF component shows no significant pulse variation and is attributed to emission from the accretion disk.

Subject headings: binaries: eclipsing — pulsars: individual (LMC X-4) — stars: neutron — X-rays: stars

1. INTRODUCTION

The orbital decay rate of an X-ray binary is an important clue to the state of its evolution (see, e.g., van den Heuvel 1983; Levine et al. 1993). Orbital decay rates have been measured for the binary X-ray pulsars Cen X-3 (Kelley et al. 1983; Nagase et al. 1992), Her X-1 (Deeter et al. 1991) and SMC X-1 (Levine et al. 1993). Measurements of LMC X-4 (Levine et al. 1991) and 4U 1538−52 (Corbet, Woo, & Nagase 1993) yielded only upper limits on the decay rates. A principal aim of the present study was to obtain with the *Ginga* and *ROSAT* X-ray satellites new pulse-timing measurements of LMC X-4 that could be combined with the earlier data for a determination of its orbital decay rate. A similar study has been reported by Safi-Harb, Ögelman, & Dennerl (1996) based on the same *ROSAT* data used herein. We also aimed to study change of the pulse period and the pulse-phase resolved spectra to obtain information about the geometry of the system and the pattern of its X-ray emission.

LMC X-4 is an eclipsing high-mass disk-fed accretion-powered binary X-ray pulsar in the Large Magellanic Cloud. First mentioned in the second *Uhuru* catalog (Giacconi et al. 1972), its optical counterpart was identified by Sanduleak & Philip (1977), and its eclipsing nature was discovered by Li, Rappaport, & Epstein (1978) and by White (1978). The X-ray intensity varies by a factor of $\sim$60 between high and low states with a periodic cycle time of 30.3 day (Lang et al. 1981). This long-term variation, like the long-term variation of Her X-1, has been attributed to blockage of the direct X-ray beam by its precessing accretion disk, which is tilted with respect to the orbit plane of the binary and periodically lies in a plane containing the line of sight to the neutron star (e.g., Lang et al. 1981; Priedhorsky & Holt 1987; Woo, Clark, & Levine 1995). About once per day LMC X-4 exhibits a "flaring episode" during which the intensity increases sporadically by factors of up to $\sim$20 for times ranging from $\sim$20 s to 45 minutes (Epstein et al. 1977; White 1978; Skinner et al. 1980; Kelley et al. 1983; Pietsch et al. 1985; Dennerl 1989; Levine et al.

[1] Harvard-Smithsonian Center for Astrophysics, 60 Garden Street, MS 70, Cambridge, MA 02138.
[2] Department of Physics, Massachusetts Institute of Technology, Cambridge, MA 02139.
[3] Universities Space Research Association.

1991). The average spectrum ($E > 1$ keV) during a flaring episode is much softer than the average spectrum at other times.

Kelley et al. (1983) discovered periodic pulsations ($P \approx 13.5$ s) in data collected during flare events. *EXOSAT* observations (Pietsch et al. 1985) demonstrated that the 13.5 s pulsations can be detected during nonflaring out-of-eclipse times. Detailed pulse-timing analyses have been carried out by Dennerl (1989) of two (1983 and 1986) *EXOSAT* observations, and by Levine et al. (1991) of a 1989 *Ginga* observation. Levine et al. (1991) combined the available times of orbital phase zero (including the result from our preliminary analysis of the 1988 *Ginga* data discussed here) to set an upper limit on the rate of orbital decay.

The observations are described in § 2 and the analysis in § 3. Interpretation and discussion of the results are presented in § 4, and a summary in § 5.

2. OBSERVATIONS

LMC X-4 was observed in its high state from 1988 March 7–10 with the LAC proportional counters on the *Ginga* satellite (Makino et al. 1987; Turner et al. 1989). The LAC counters had a 1°.1 × 2°.0 FWHM field of view and a total effective area of 4000 cm^2. The intrinsic energy resolution of the LAC detectors was 20% FWHM at 5.9 keV. The data were accumulated in the MPC 1H, MPC 2L, MPC 2M, or MPC 2H mode, which provided 48 channel pulse-height distributions (PHDs) in the form of counts per channel per second with time resolutions of 0.0625, 0.5, or 2.0 s. The observation began at orbital phase 0.5 and lasted for 2.3 orbital cycles with the usual gaps due to Earth blockages and trapped particle interference.

The *Ginga* data were corrected for background according to the algorithm of Hayashida et al. (1989) that describes the magnitude and orbital variation of the energetic charged-particle–induced contribution to the PHDs. To remove the background due to diffuse X-rays and other sources in the field of view we subtracted the average deep-eclipse PHD from each of the accumulated PHDs. This procedure also subtracted the PHD of X-rays from LMC X-4 in eclipse that arrive by scattering from circumstellar matter. However, the spectrum of these scattered X-rays is similar to that of the out-of-eclipse X-rays, and their flux is only ~0.5% of the out-of-eclipse flux. Thus this background-subtraction procedure did not significantly distort the resulting PHD of the uneclipsed LMC X-4.

Another high-state observation of LMC X-4 was made from 1991 October 28.6 to November 3.6 with the Position Sensitive Proportional Counter (PSPC) in the focal plane of the X-ray Telescope (XRT) of the *ROSAT* X-ray observatory (Trümper 1983). The PSPC-XRT system (Pfeffermann et al. 1987; Aschenbach 1988) was sensitive to X-rays in the energy range from 0.1 to 2.5 keV and had a field of view of 57′ radius. The energy resolution of the PSPC was 45% FWHM at 1 keV. The PSPC-XRT system recorded for each detected photon the arrival direction with an angular resolution of ~25″ and the arrival time to ~0.1 ms. The observation yielded 46,000 s of useful data. Its primary purpose was to observe the northern part of the Large Magellanic Cloud; LMC X-4 was located about 40′ away from the image center (Bomans, Dennerl, & Kürster 1994).

The *ROSAT* image of LMC X-4 was relatively large because of the off-axis aberration of the XRT. We therefore accepted counts from a circular source region of radius 4′.5 centered on the image of LMC X-4. Only events in pulse-height channels 20–249 (0.2–2.5 keV) were used. To correct for background in the spectrum analysis, we subtracted from each PHD of the source region a background PHD evaluated from the total counts in a concentric annulus with inner and outer radii of 6′ and 8′, scaled according to the number of pixels.

3. DATA ANALYSIS AND RESULTS

3.1. *Temporal Analysis*

Pulse-timing analyses were carried out separately on the two sets of data from the *Ginga* and *ROSAT* observations. The times of each accumulation bin of the *Ginga* data and of each photon detection in the *ROSAT* data were corrected for the arrival time delay at Earth relative to the solar system barycenter. The *ROSAT* data were then binned in 0.1 s intervals so that they could be analyzed with the same software as the binned data from *Ginga*. For the timing analysis of the *Ginga* observation we used the data in the pulse-height channels corresponding to energies below 9.3 keV because this energy band yielded the least root mean square difference between the observed pulse arrival times and the predicted arrival times derived from the final timing solution.

Dealing with each of the *Ginga* and *ROSAT* data sets separately, and using for each set the binary orbital parameters extrapolated from the values determined from earlier observations by Levine et al. (1991), we adjusted the barycentric bin times according to the orbital motion of the pulsar so as to achieve a first approximation to an elimination of orbital variations in the pulse arrival times. We then grouped the data into subsets of sufficiently short duration so that they could be folded with a trial intrinsic pulse period without significant smearing of the pulse profile. Subsets containing clear evidence of an X-ray flare were rejected. The data in each subset were folded with an estimated value of the intrinsic pulse period to obtain a pulse profile, and a template profile was formed by summation of the subset profiles. The template was cross-correlated with each of the subset profiles to reveal deviations in pulse phase. A linearized model was fitted to the deviations to obtain corrections to the intrinsic pulse period and to the orbital parameters. The entire analysis process was then repeated using the adjusted pulse period and orbital parameters beginning with the step in which the bin times are corrected for the binary motion. Several iterations sufficed to yield a stable set of best-fit orbital parameters and intrinsic pulse period.

The filled circles in Figures 1*a* and 1*b* indicate the measured pulse arrival time delays with the effects of the binary orbital motion included (i.e., we show the delays for the best-fit orbit summed with the differences between the measurements and the best-fit model). The smooth curve is a plot of the delays predicted for a circular orbit with the best-fit binary parameters that are summarized in Table 1. The differences between the observed and predicted delays, indicated by the crosses, have rms values of 0.072 s and 0.364 s for the *Ginga* and *ROSAT* data, respectively.

The intrinsic pulse periods derived from our two data sets are plotted against time in Figure 2 along with the pulse periods determined from previous observations. The average rate of change of the pulse period between the 1988

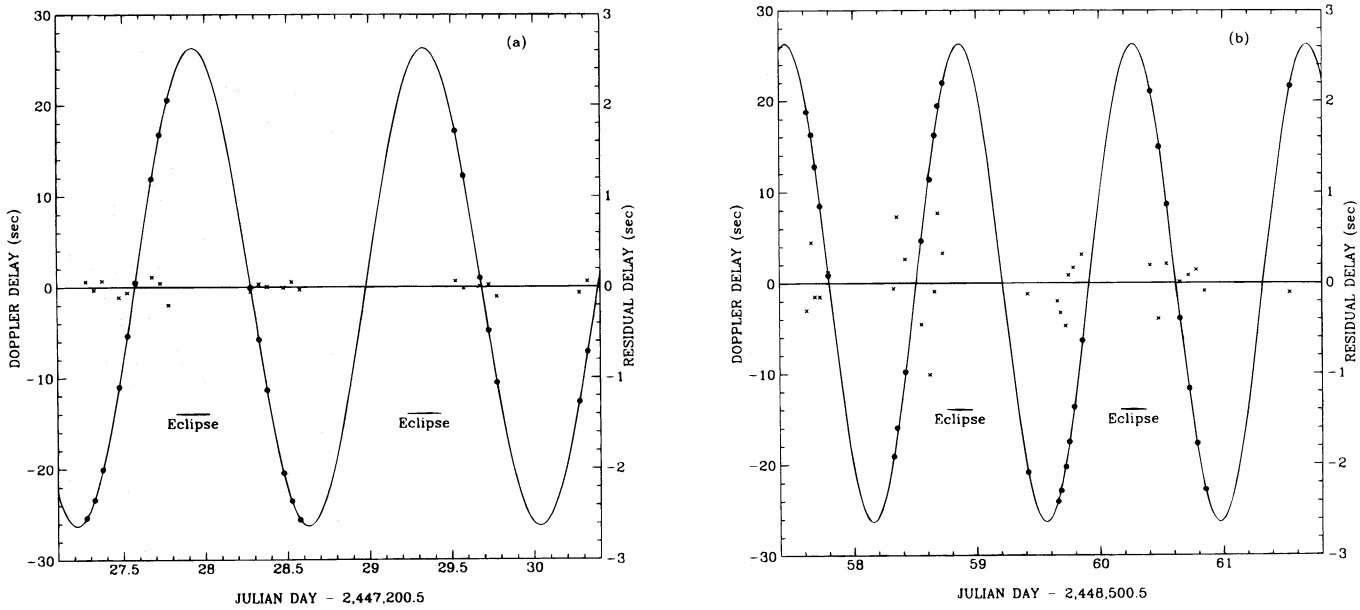

FIG. 1.—Doppler delay data for LMC X-4 derived from *Ginga* observations in 1988 March (*a*) and *ROSAT* observations in 1991 (*b*). The filled circles indicate the differences between the measured pulse arrival times and the expected arrival times of pulses with a constant period equal to the average period of the observed pulses. The smooth curve is the fitted curve of Doppler delays for a circular orbit. The crosses indicate the residuals (*right-hand scale*) of the fit.

TABLE 1

PARAMETERS FOR THE LMC X-4 BINARY SYSTEM

Parameter	*Ginga* Value	1 σ	*ROSAT* Value	1 σ
$a_x \sin i$ (lt-s)[a]	26.27	0.04	26.20	0.19
Eccentricity[a]	0.006	0.003	0.008	0.014
T_0[a] (eclipse center; barycentric)	JD 2447229.8313	0.0004	JD 2448559.3598	0.0013
P_{pulse}[a] (barycentric) (s)	13.495978	0.000009	13.50292	0.00002
M_x ($M_\odot$)[b]	1.38	0.25		
M_c ($M_\odot$)[b]	14.7	2.0		
R_c ($R_\odot$)[b]	7.6	0.8		
Inclination angle (deg)[b]	68	6		
$\theta_{eclipse}$ (deg)[b]	26–28			

[a] Derived from the *Ginga* and *ROSAT* observations.
[b] Levine et al. 1991 and references therein.

Ginga and the 1991 *ROSAT* observations was $\dot{P}_{pulse} = (1.91 \pm 0.01) \times 10^{-3}$ s yr^{-1}.

The present and previous determinations of epochs of orbital phase zero (eclipse center) are shown in Figure 3 in the form of a plot against orbit number of the differences between the measured times of phase zero and the time predicted from the best-fit constant orbital period of 1.40840212 days. The dashed curve is the weighted least-squares fit of a quadratic function (see Table 2 for the fitted parameters). The coefficient of the quadratic term of the fitting function implies a value of $\dot{P}_{orb}/P_{orb} = (-5.3 \pm 2.7) \times 10^{-7}$ yr^{-1} for the rate of change of the orbital period. If the *SAS 3* determination is omitted, we obtain a value of $\dot{P}_{orb}/P_{orb} = (-6.0 \pm 2.8) \times 10^{-7}$ yr^{-1}.

TABLE 2

ORBITAL FITS FOR THE *Ginga* AND *ROSAT* OBSERVATIONS

Parameter	Value	Uncertainty (1 σ)
a_0 (JD)[a]	JD 2446729.84878	0.0041
a_1 (days)[a]	1.40840249	6.0×10^{-7}
a_2 (days)[a]	-1.45×10^{-9}	0.72×10^{-9}
$\dot{P}_{orb}/P_{orb}$ (per year)	-5.3×10^{-7}	2.7×10^{-7}

[a] The time of the nth eclipse can be written as $t_N = a_0 + a_1 N + a_2 N^2$.

3.2. *Spectrally Resolved Pulse Profiles*

Figure 4 displays the pulse-height resolved pulse profiles that we derived by folding the Doppler-corrected data by the intrinsic pulse period. The phase of the *ROSAT* profiles was adjusted to maximize the cross correlation between the 1.2–2.3 keV *Ginga* profile and the 1.0–2.4 keV *ROSAT* profile.

The low- and high-energy profiles have single peaks that are 180° out of phase with respect to one another. Their pulse fractions, defined as $(I_{max} - I_{min})/I_{max}$, are both $\sim$0.13. The complex profile in the intermediate-energy range from 4.7 to 9.9 keV is double peaked with a pulse fraction of $\sim$0.07 and has features with phase widths less than 0.03. We note that these profiles are similar to those obtained from an observation of LMC X-4 with *Ginga* in 1989 (Levine et al. 1991).

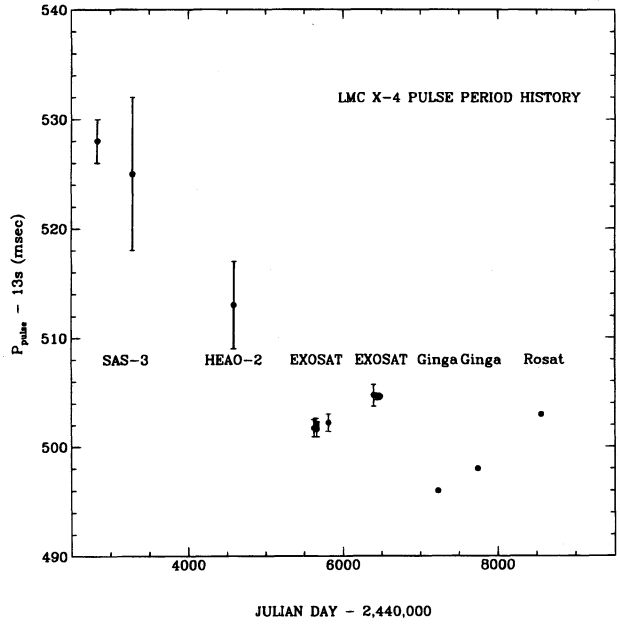

FIG. 2.—Pulse period history of LMC X-4. The *SAS 3*, *HEAO 2*, *EXOSAT*, *Ginga*, and *ROSAT* data are from Kelley et al. (1983), Naranan et al. (1985), Dennerl (1989b), Levine et al. (1991), and the present work. All of these measurements have been corrected for the orbital motion of the pulsar.

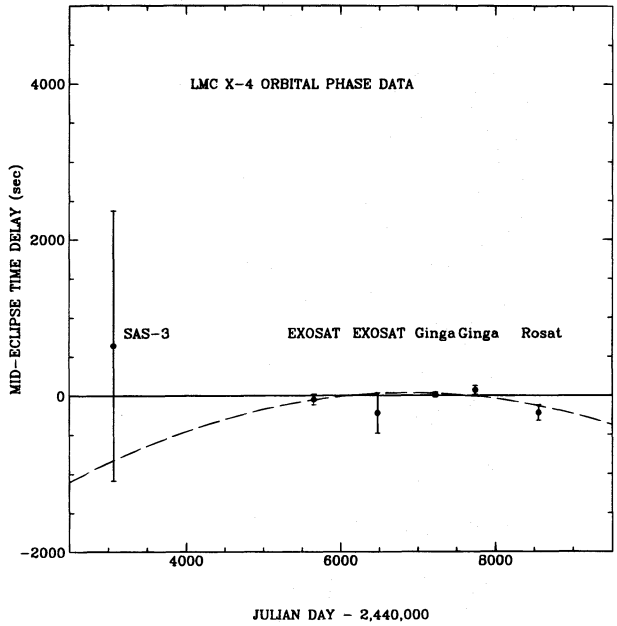

FIG. 3.—Summary of mid-eclipse times of LMC X-4. The *SAS 3*, *EXOSAT*, *Ginga*, and *ROSAT* data are from Li, Rappaport, & Epstein (1978), Dennerl (1989b), Levine et al. (1991), and the present work. The filled circles indicate the differences between measured times of mid-eclipse (orbit phase 0) and times predicted for a constant orbital period of ($P = 1.4084021$ days), equal to the overall average period. The dashed curve is a quadratic fit to the data.

3.3. *Pulse-Phase Resolved Spectroscopy*

We have simultaneously fitted the *ROSAT* and *Ginga* PHDs by a multicomponent spectral model using the XSPEC Spectral Fitting Package of the Goddard Space Flight Center and instrument response matrices furnished by the *ROSAT* and *Ginga* Data Centers. To achieve satisfactory fits over the wide energy range covered by the combined data we found it sufficient to include a Planck function (PF), thermal bremsstrahlung (TB), a power law (PL), and a Gaussian-shaped iron emission line (FE). The sum of these components was multiplied by a photoelectric

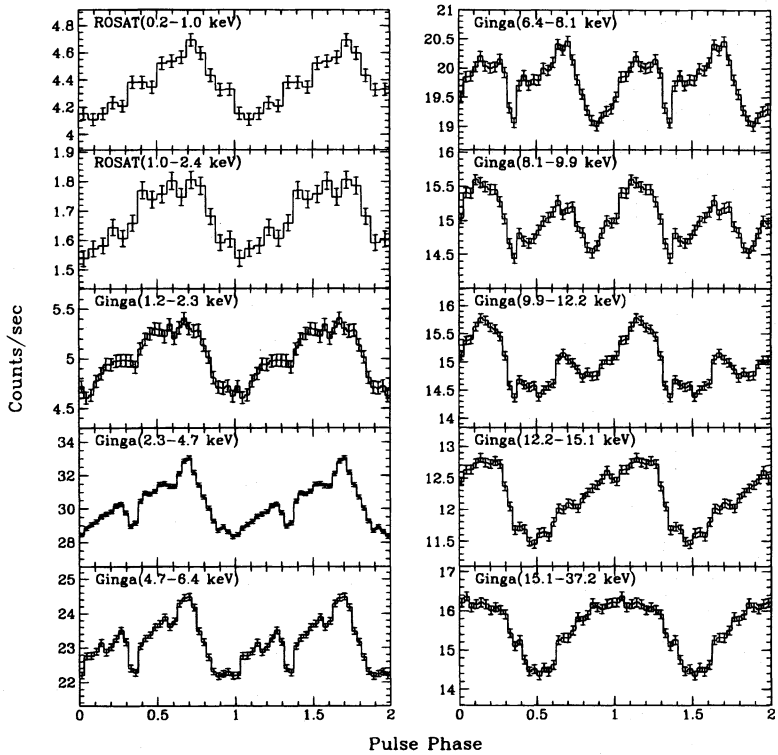

FIG. 4.—Pulse profiles of LMC X-4 from the *ROSAT* and *Ginga* observations. The pulse profiles from the *ROSAT* observation are binned in 16 phase bins (~0.84 s time bins) and those from the *Ginga* observation are binned in 32 phase bins (~0.42 s time bins). The phase of the *ROSAT* pulse profiles has been adjusted to match the phase of the 1.0–2.4 keV *ROSAT* profile to the 1.2–2.3 keV *Ginga* profile.

absorption factor, an exponential high-energy cutoff, and a cyclotron resonance high-energy attenuation factor (all energies expressed in keV):

$$I(E) = \exp\left[-\sigma(E)N_{\rm H}\right] \times \left[f_{\rm PF}(E) + f_{\rm TB}(E) + f_{\rm PL}(E) + f_{\rm FE}(E)\right] f_{hi}(E) f_{\rm cy}(E)\,, \quad (1)$$

where

$$f_{\rm PF}(E) = I_{\rm PF}\left(\frac{E}{E_{\rm PF}}\right)^2 (e-1)\left[\exp\left(\frac{E}{E_{\rm PF}}\right) - 1\right]^{-1},$$

$$f_{\rm TB}(E) = I_{\rm TB}\exp\left(-\frac{E}{E_{\rm TB}}\right)\frac{G(E, E_{\rm TB})}{E},$$

$$f_{\rm PL}(E) = I_{\rm PL}E^{-\alpha},$$

$$f_{\rm FE}(E) = I_{\rm FE}(2\pi\sigma_{\rm FE}^2)^{-1/2}\exp\left[-\frac{(E-E_{\rm FE})^2}{2\sigma_{\rm FE}^2}\right],$$

$$f_{hi}(E) = \begin{cases} 1\,, & E < E_c \\ \exp\left(-\dfrac{E-E_c}{E_f}\right), & E \geq E_c \end{cases},$$

$$f_{\rm cy}(E) = \exp\left[-\frac{A_{\rm cy}W_{\rm cy}^2(E/E_{\rm cy})^2}{(E-E_{\rm cy})^2 + W_{\rm cy}^2}\right].$$

In these equations $I_{\rm PF}$ is the Planck function intensity at 1 keV and e is the base of natural logarithms; $f_{\rm TB}(E)$ is the TB model defined by XSPEC with two fitting parameters: temperature $E_{\rm TB}$ and normalization factor $I_{\rm TB}$; $G(E, E_{\rm TB})$ is the Gaunt factor at energy E for a plasma of temperature $E_{\rm TB}$ keV; $I_{\rm PL}$ is the power-law intensity at $E = 1$ keV; $I_{\rm FE}$ is the total iron line intensity. We ignored the effects of X-ray ionization on the attenuation cross section for the column density measurement and assumed it to be $\sigma(E) = \sigma_{\rm ph}(E) + 1.21\sigma_{\rm T}$, where $\sigma_{\rm ph}(E)$ is the photoelectric absorption cross section of cold matter given by Morrison & McCammon (1983) and $\sigma_{\rm T}$ is the Thomson scattering cross section.

Our analysis assumes that both the intensity and shape of the spectrum of LMC X-4 may vary with pulse phase, but that longer term variations are simply changes in the overall intensity. To test for a possible change in the average flux of LMC X-4 between the *ROSAT* and *Ginga* observations and for systematic errors in the relative calibration of the two instruments, we compiled the total PHDs of the *ROSAT* and *Ginga* data sets (see Fig. 5). To the statistical error in the counting rate of each pulse-height channel we added in quadrature an estimated 1% systematic error. We then fitted the two PHDs simultaneously with a normalization factor of the *Ginga* data free to vary.

The resulting best-fit spectral function and its four components are plotted in Figure 6. Table 3 lists the fitted parameters. The Planck component (*dashed line*) dominates the low-energy end of the spectrum, the power-law component (*dotted line*) dominates the high-energy end of the spectrum, and the thermal bremsstrahlung component (*dash-dotted line*) dominates the intermediate range between the Planck and power-law components. Fits of comparable quality are obtained with any combination of PF and TB functions as models for the low and intermediate range of energies. Much worse fits are obtained with only one component. Our choice of the particular combination of PF and TB is motivated by our physical interpretation as discussed in § 4. Of course, no simple function representing a model of a complex X-ray source can be expected to yield a perfect fit to data of high statistical precision like that of the present data. Therefore, it is not surprising that the formal reduced χ^2 value of the fit we have obtained is substantially larger than unity.

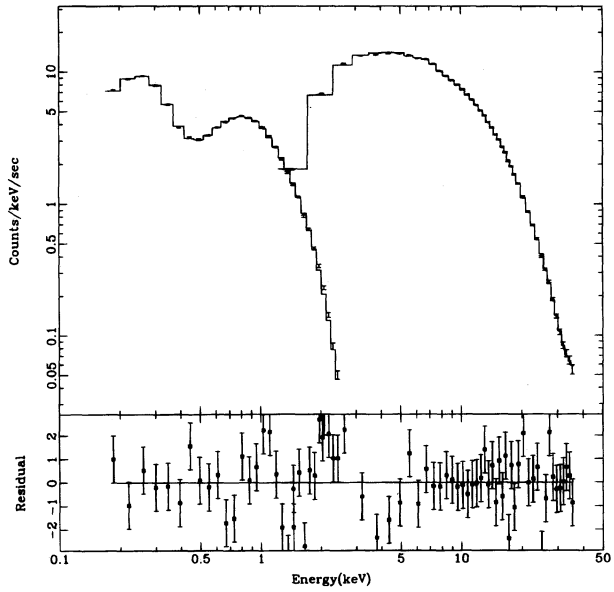

FIG. 5.—Combined pulse-height distributions (PHDs) of the pulse-averaged data from the *Ginga* and *ROSAT* observations. The solid histograms are the computed PHDs derived from the model spectrum with fitted parameters. The different normalizations of the data are taken into account in the instrument response functions employed by the spectral fitting program.

The value of the relative normalization factor that yielded the minimum χ^2 was 0.98, fortuitously close to unity in view of the well-known variability of the source. This factor was applied to the *Ginga* data in the analysis of the pulse-phase resolved PHDs. The column density in the photoelectric

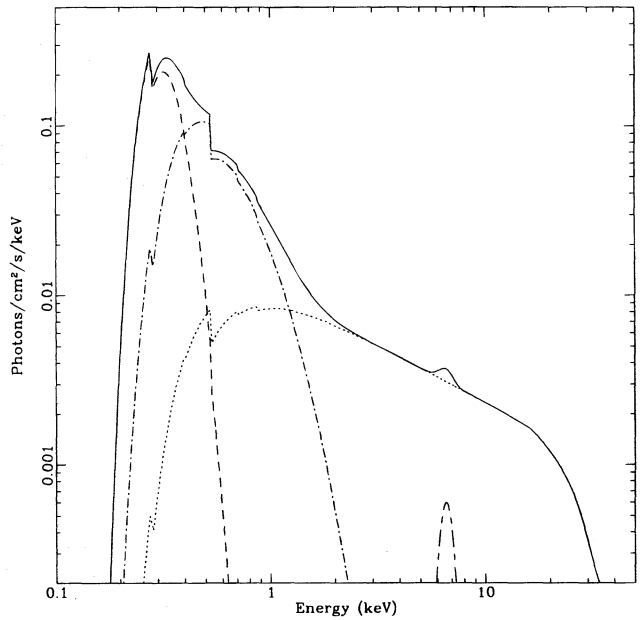

FIG. 6.—Plot of the four components of the spectrum and their sum that were fitted simultaneously to the *Ginga* and *ROSAT* pulse height distribution displayed in Fig. 5. The components are comprised of a Planck function (*dashed line*), thermal bremsstrahlung (*dash-dotted line*), power law (*dotted line*), and iron K-line emission (*long-short dashed line*).

TABLE 3

FITTED VALUES OF THE SPECTRAL FUNCTION

Parameter	Value	Uncertainty (1 σ)
N_H (10^{20} cm^{-2})	11.4	0.5
E_{PF} (keV)	0.0299	0.0013
I_{PF} (photons keV^{-1} cm^{-2} s^{-1})	894	498
E_{TB} (keV)	0.354	0.011
I_{TB} (photons cm^{-2}s^{-1})	0.375	0.037
α	0.669	0.008
I_{PL} (photons keV^{-1} cm^{-2} s^{-1})	0.0110	0.0002
E_c (keV)	16.1	0.4
E_f (keV)	35.6	6.7
A_{cy}	1.15	0.17
E_{cy} (keV)	33.7	0.6
W_{cy} (keV)	8.3	1.2
E_{FE} (keV)	6.59	0.06
σ_{FE} (keV)	0.47	0.09
I_{FE} (photons cm^{-2} s^{-1})	0.00070	0.00008
N_{Ginga}/N_{ROSAT}[a]	0.98	0.02
χ^2_ν	2.1	...

[a] Relative normalization ratio of *Ginga* PHD to *ROSAT* PHD.

absorption factor from the best-fit phase-averaged spectrum was also fixed for the analysis of the pulse-phase resolved PHDs, while the values of all the other fitting parameters were allowed to vary. The variation with pulse phase of the shape and normalization parameters of the four components of the model spectrum is displayed in Figure 7.

The energy fluxes of the four spectral components, derived from the fitted parameters, are plotted against pulse phase in Figure 8. The TB and PL ($E > 15$ keV) flux profiles have single peaks with pulse fractions of $\sim$12% and $\sim$16%, respectively, which are 180° degrees out of phase with one another. The iron line flux varies with a significantly larger pulse fraction of $\sim$37% and its maximum lags by $\sim$140° that of the high-energy flux which is presumably responsible for its excitation. There is no significant broad pulse variation in the flux of the low-energy component represented by the Planck function, although the statistical uncertainties are large enough to hide a pulse fraction as large as that of the TB and PL components.

4. DISCUSSION

4.1. *Orbital Period Change*

The values of $\dot{P}_{orb}/P_{orb}$ for three massive binary X-ray pulsars LMC X-4 are listed in Table 4. Although the value for LMC X-4 we have found must be considered as marginal evidence for actual decay, it definitely establishes that the decay rate is substantially less than that of Cen X-3 and SMC X-1. We note that the analysis of Safi-Harb et al. (1996) utilized early determinations of eclipse centers derived from optical data but was otherwise based on the same set of measurements (including the time of orbital phase zero derived from *Ginga* data that we present here) as our result. They obtained approximately the same value for the rate of orbital decay, but claim that the estimated uncertainty in $\dot{P}_{orb}/P_{orb}$ is $\pm 0.5 \times 10^{-7}$ yr^{-1}. When those optical

TABLE 4

MEASURED ORBITAL DECAY RATES OF MASSIVE X-RAY BINARIES

Name	Orbital Period Changes ($\times 10^{-7}$ yr^{-1})	References
Cen X-3	$\dot{P}_{orb}/P_{orb} = -17.38 \pm 0.04$	1
SMC X-1	$\dot{P}_{orb}/P_{orb} = -33.6 \pm 0.2$	2
LMC X-4	$\dot{P}_{orb}/P_{orb} = -5.3 \pm 2.7$	3
4U 1538−52	$\lvert\dot{P}_{orb}/P_{orb}\rvert < 60$	4, 5

References. (1) Nagase et al. 1992; (2) Levine et al. 1993; (3) present work; (4) Cominsky & Moraes 1991; (5) Corbet et al. 1992.

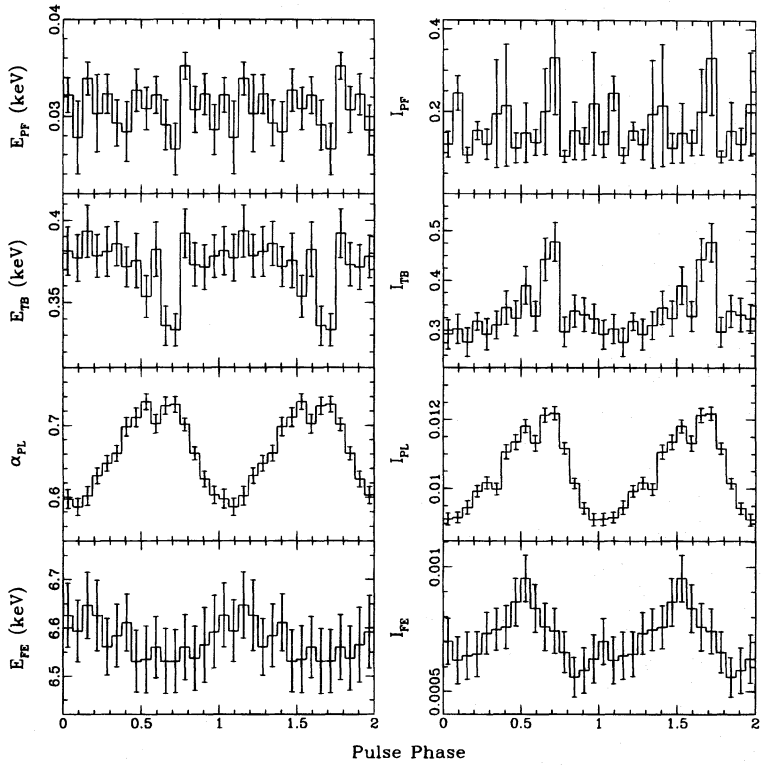

FIG. 7.—Plots against pulse phase of the shape and normalization parameters of the four components of the model spectrum (eq. [1]) fitted simultaneously to the *Ginga* and *ROSAT* pulse-phase resolved pulse-height distributions.

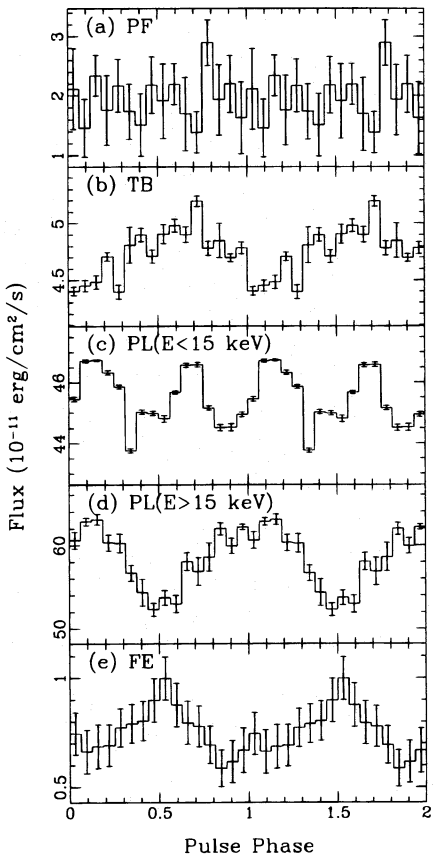

FIG. 8.—Plots against pulse phase of the energy fluxes in the energy range from 0.2 to 40 keV of the four spectral model components: Planck function (PF), thermal bremsstrahlung (TB), power-law function (PL), and iron line (FE). The error bars for each component indicate the range of flux values obtained by fixing the corresponding normalization factor at the 1 σ limits given by XSPEC program and then refitting the model.

data are included in our analysis we find only a small decrease in the estimated error from $\pm 2.7 \times 10^{-7}$ yr^{-1} to $\pm 2.4 \times 10^{-7}$ yr^{-1}. We believe that our error estimate is correct and that the stated uncertainty of Safi-Harb et al. (1996) is a substantial underestimate.

The large orbital decay rate in SMC X-1 and the large radius of its companion Sk 160 ($14 < R < 20\ R_\odot$) led Levine et al. (1993) to the conclusion that Sk 160 is expanding rapidly as it burns hydrogen in a shell. The resulting rapid increase in the moment of inertia acts to reduce the rotation rate of the companion, producing a relatively large difference between the stellar rotation and orbital angular frequencies. This enhances the loss of energy by tidal friction, which can produce a large orbital decay rate.

Compared to SMC X-1, the orbital decay rate of the LMC X-4 system is much lower and the companion much smaller ($7 < R < 9\ R_\odot$). Safi-Harb et al. (1996) have noted that conservative mass transfer alone would cause an orbital period change of $\dot{P}_{\rm orb}/P_{\rm orb} = -1 \times 10^{-7}$ yr^{-1}. Angular momentum loss through mass loss could produce a somewhat higher orbital decay rate. Each of the three effects—tidal friction, conservative mass transfer, and mass loss—may be contributing to orbital decay in LMC X-4. When the possible contributions to the orbital decay rate from mass transfer and mass loss, and the relatively large uncertainty in the measured decay rate, are taken into account, the contribution of tidal friction to the decay rate is rather uncertain. However, the range of possible values of the tidal friction contribution and the measured size of the companion star are quantitatively consistent with the expected size and rate of expansion of a companion that is burning hydrogen in its core during its evolution on the main sequence. If the tidal friction contribution is small, the companion could be in the early part of its evolution; if it is large, it is likely to be in the later stages of its life on the main sequence.

4.2. *Spin Period Change*

The spin-period history of LMC X-4 (Fig. 2) shows episodes of spin acceleration and deceleration with average values of $\dot{P}_{\rm pulse}$ ranging from -4.0×10^{-3} s yr^{-1} between the *HEAO 2* and first of the *EXOSAT* observations, to 1.9×10^{-3} s yr^{-1} between the most recent *Ginga* and *ROSAT* observations. Thus it is likely that LMC X-4 is near the condition of spin equilibrium that occurs when the spin period equals the Kepler period near the inner boundary of the accretion disk. According to the theory of disk-fed accretion (see Ghosh & Lamb 1979), a pulsar in spin equilibrium that has the high luminosity of LMC X-4 and its spin period of $\sim$13.5 s must have an exceptionally high magnetic dipole moment, of the order of $10^{31.5}$ G cm^3, in order to maintain the inner boundary of the accretion disk at a radius with so large a Kepler period. A similar conclusion was previously drawn by Naranan et al. (1985).

4.3. *Pulse-Phase Dependent Spectral Properties*

As a first approximation, the directional variation of X-ray emission by an X-ray pulsar can be modeled by a superposition of an isotropic component, two pencil-like beams oppositely directed and aligned with cylindrical symmetry about the magnetic dipole axis, and a cylindrically symmetric fanlike beam with its maximum in the plane perpendicular to the dipole axis. It seems plausible to associate the fan beam with emission from the sides of the accretion columns, and the pencil beams with emission from the impact areas of accretion near the surface of the neutron star. If Θ is the inclination of the spin axis, and Φ the angle between the spin and dipole axis, then the condition that a pencil or a fan beam, by itself, produces a single-peak pulse profile is $\Theta + \Phi < 90°$ (Clark et al. 1990 and references therein).

The pulse profiles of the TB and PL ($E > 15$ keV) intensities shown in Figure 8 are both single peaked, but approximately 180° out of phase with one another. Thus a first-approximation model of the X-ray emission is a combination of a pencil and a fan beam under the angle constraint required for single peaks. It seems likely that the high-energy component of a pulsar spectrum would be emitted from the impact area of the accretion flow and would be broadly collimated as a pencil beam in the direction perpendicular to the surface of the neutron star. Therefore we attribute the gross features of the profiles to a power-law pencil beam and a thermal bremsstrahlung fan beam. The narrow features evident in the TB and PL ($E < 15$ keV) profiles show the presence of additional and more sharply collimated beams in the emission pattern. The fact that the iron-line component has a well-defined single-peak profile suggests that the iron line X-rays are emitted by matter corotating with the pulsar. On the other hand, the phase lag and the fact that its pulse fraction appears to be significantly larger than that of the X-rays responsible for its excitation suggest that a mechanism involving variable

illumination of the accretion disk may be the cause of the iron-line pulse profile. In that case, one might expect to see a variation of the phase lag between the high-energy component and the iron-line component as the accretion disk precesses with its 30 day period.

Finally, we note that if the low-energy flux, modeled by the Planck function, is actually emission from the accretion disk, one would not expect it to vary with the pulse phase. Unfortunately, the statistical uncertainties in the low-energy flux pulse profile are too large to yield a significant test of this origin.

5. SUMMARY

Pulse-timing and pulse-phase resolved spectral analysis of *Ginga* and *ROSAT* observations of LMC X-4 in 1988 and 1991, respectively, have led to the following conclusions:

1. The rate of change of the orbital period, derived from these observations and previous X-ray observations dating back to 1977, is $\dot{P}_{\rm orb}/P_{\rm orb} = (-5.3 \pm 2.7) \times 10^{-7}$ yr^{-1}. This rate, which is small compared to that of Cen X-3 and SMC X-1, places a low limit on the rate of orbital energy dissipation by tidal friction. Together with the relatively small radius of the companion, it is evidence that the companion is still burning hydrogen in its core.

2. The spin period increased at an average rate of $\dot{P}_{\rm pulse} = (1.91 \pm 0.01) \times 10^{-3}$ s yr^{-1} between the *Ginga* and *ROSAT* observations. Since the spin period is observed at various times to increase and decrease, the pulsar must be near a state of equilibrium wherein its spin period approximately equals the Kepler period at the inner edge of the accretion disk. For such a condition to hold for a pulsar with the high luminosity of LMC X-4 and a spin period of $\sim$13.5 s, the magnetic dipole strength must be exceptionally high, of the order of $10^{31.5}$ G cm^3.

3. The gross features of the pulse-phase modulation of the X-ray emission can be modeled as the sum of three components: a high-energy component ($E > 15$ keV) represented by a power law with index $\alpha \sim 0.7$ (with a high-energy cutoff) emitted in a broad pencil beam aligned with the magnetic dipole axis, a thermal bremsstrahlung component with temperature $kT \sim 0.35$ keV emitted in a fan beam perpendicular to the dipole axis, and an iron line at $E \sim 6.6$ keV emitted either by material corotating with the pulsar or by the accretion disk scanned by the pencil beam. In addition, the spectrum fit requires the presence of a low-energy pulse-phase independent component that can be modeled as steady Planck emission from the accretion disk with an effective temperature of 0.03 keV.

This research was supported in part by Grants NAG 8-701, NAG5-1656 & NAG8-288 from the National Aeronautics and Space Administration.

REFERENCES

Aschenbach, B. 1988, Appl. Opt., 27, No. 8, 1404
Bomans, D. J., Dennerl, K., & Kürster, M. 1994, A&A, 283, L21
Clark, G. W., Woo, J. W., Nagase, F., Makishima, K., & Sakao, T. 1990, ApJ, 353, 274
Cominsky, L. R., & Moraes, F. 1991, ApJ, 370, 670
Corbet, R. H. D., Woo, J. W., & Nagase, F. 1993, A&A, 276, 52
Deeter, J. E., Boynton, P. E., Miyamoto, S., Kitamoto, S., Nagase, F., & Kawai, N. 1991, ApJ, 383, 324
Dennerl, K. 1989, Ph.D. thesis, Max-Planck-Institut für Extraterrestrische Physik
Epstein, A., Delvaille, J., Helmken, H., Murray, S., Schnopper, H., Doxsey, R., & Primini, F. 1977, ApJ, 216, 103
Ghosh, P., & Lamb, F. K. 1979, ApJ, 234, 296
Giacconi, R., Murray, S., Gursky, H., Kellogg, E., Schreier, E., & Tananbaum, H. 1972, ApJ, 178, 281
Hayashida, K., et al. 1989, PASJ, 41, 373
Kelley, R. L., Jernigan, J. G., Levine, A., Petro, L. D., & Rappaport, S. 1983, ApJ, 264, 568
Lang F. L., et al. 1981, ApJ, 246, L21
Levine, A., Rappaport, S., Deeter, J. E., Boynton, P. E., & Nagase, F. 1993, ApJ, 410, 328
Levine, A., Rappaport, S., Putney, A., Corbet, R., & Nagase, F. 1991, ApJ, 381, 101
Li, F., Rappaport, S., & Epstein, A. 1978, Nature, 271, 37
Makino, F., & the ASTRO-C Team, 1987, Ap. Lett. Comm., 25, 223
Morrison, R., & McCammon D. 1983, ApJ, 270, 119
Nagase, F., Corbet, R. H. D., Day, C. S. R., Inoue, H., Takeshima, T., & Yoshida, K. 1992, ApJ, 396, 147
Naranan, S., et al. 1985, ApJ, 290, 487
Pfeffermann, E., et al. 1987, Proc. SPIE, 733, 519
Pietsch, W., Pakull, M., Voges, W., & Staubert, R. 1985, Space Sci. Rev., 40, 371
Priedhorsky, W. C., & Holt, S. S. 1987, Space Sci. Rev., 45, 291
Safi-Harb, S., Ögelman, H., & Dennerl, K. 1996, ApJ, 456, L37
Sanduleak, N., & Philip, A. G. D. 1977, IAU Circ., No. 3023
Skinner, G. K., et al. 1980, ApJ, 240, 619
Trümper, J. 1983, Adv. Space Res., 2, No. 4, 241
Turner, M., et al. 1989, PASJ, 41, 345
van den Heuvel, E. P. J. 1983, in Accretion Driven Stellar X-Ray Sources, ed. W. H. G. Lewin & E. P. J. van den Heuvel (Cambridge: Cambridge Univ. Press), 303
White, N. E. 1978, Nature, 271, 38
Woo, J. W., Clark, G. W., & Levine, A. M. 1995, ApJ, 449, 880